

Virtual Memory for 3D Gaussian Splatting

Jonathan Haberl , Philipp Fleck , and Clemens Arth 

Abstract—3D Gaussian Splatting represents a breakthrough in the field of novel view synthesis. It establishes Gaussians as core rendering primitives for highly accurate real-world environment reconstruction. Recent advances have drastically increased the size of scenes that can be created. In this work, we present a method for rendering large and complex 3D Gaussian Splatting scenes using virtual memory. By leveraging well-established virtual memory and virtual texturing techniques, our approach efficiently identifies visible Gaussians and dynamically streams them to the GPU just in time for real-time rendering. Selecting only the necessary Gaussians for both storage and rendering results in reduced memory usage and effectively accelerates rendering, especially for highly complex scenes. Furthermore, we demonstrate how level of detail can be integrated into our proposed method to further enhance rendering speed for large-scale scenes. With an optimized implementation, we highlight key practical considerations and thoroughly evaluate the proposed technique and its impact on desktop and mobile devices.

1 INTRODUCTION

In Novel View Synthesis (NVS), a set of pictures of a scene is taken and used to create new images. These images may be generated from arbitrary viewpoints, beyond those included in the original set of pictures. The objective is to make these synthetic images convincing; seemingly taken in the original scene. One popular method is 3D Gaussian Splatting (3DGS). In 3DGS, Gaussians are modified until virtual, rendered images match real pictures closely. These Gaussians are powerful descriptors that can accurately represent even complex real-world environments. Figure 1 depicts such a novel view of a reconstructed scene using 3DGS.

3DGS uses neither mesh nor texture. Its only primitive is a 3D Gaussian, while the collectivity of 3D Gaussians represents a scene accessible in Central Processing Unit (CPU) memory. As the scales of 3DGS scenes increase, so does the memory and work required to store and render them. Depending on the actual size of the scene, the amounts of data can be huge, multiple gigabytes or terabytes even. Handling 3DGS reconstructions requires graphics engines with high memory bandwidth along with huge amounts of memory, which seriously limits the application of 3DGS and puts its use on even modern mobile computers out of reach. Therefore, novel ideas and the invention of new methods to tackle these problems are of high relevance.

The method introduced in this work is concerned with these aspects of efficient data handling and rendering of large scenes. We propose the use of virtual memory and Level of Detail (LOD) which help to achieve virtually unlimited scene scale and efficient rendering, even on low-end mobile devices. At a glance, virtual memory is used to handle such amounts of data and to provide the means for efficient rendering. Gaussians that are visible from a certain viewpoint are determined as quickly as possible and then transferred to Graphics Processing Unit (GPU) memory. Thereby, Gaussians outside the view frustum or those occluded by other structures can be discarded and a significant amount of computation and memory can be saved. Through virtual textures that are continuously updated and exchanged between CPU and GPU memory, rendering large scenes, such as in open-world video games, becomes possible, even if the total size of the textures is larger than the available GPU memory. Our approach is split into two parts: a **preprocessing** and a **real-time rendering** part.

In the preprocessing stage, an existing 3DGS scene is analyzed offline to create a mesh that approximates the structure present in



Fig. 1: 3D Gaussian Splatting scene of a truck. The scene is provided by the original paper and imported and rendered in our Vulkan renderer.

the scene. Gaussians are separated into pages that group them by their proximity. Each face on the proxy mesh is marked with the corresponding page ID. Where pages overlap, links between them are established. Finally, lower LOD levels for each page are provided.

The second part of our method is concerned with rendering scenes in real time. The preprocessed scene is imported and for each frame, we first render the page IDs on the proxy mesh to a visibility buffer. The sole purpose of this buffer is to find out the IDs of pages in view of the camera. The page IDs contained in the image, as well as their established links, allow us to determine which pages of Gaussians will likely be visible. The pages are then transferred to GPU memory and rendered using a modern rendering API.

Note that we do not modify the process of scene creation. Any scene in the format described by Kerbl *et al.* [14] is compatible with the approach presented. This includes the original implementation, similar derivative implementations, and at least a subset of more recent implementations that focused on increasing the size of reconstructed scenes. Several solutions have been proposed to reduce the memory usage or modify the attributes of 3DGS scenes. Many of these modifications may generally be used in combination with our work in the future. However, we limit our exploration of such extensions to a discussion of 3DGS compression in related work.

In the following, we provide details about the concepts involved, from preprocessing to per-frame operations. We explore several alterations to the basic idea to improve quality and performance or limit memory usage and highlight the resulting trade-offs. An end-to-end implementation is provided, together with an in-depth evaluation. Our contributions can thus be summarized as follows:

- a novel approach to virtual memory and LOD within 3DGS;
- an implementation for pre-processing and real-time rendering using a modern rendering API;
- an efficient method for rendering a set of large scenes on mobiles; and
- a detailed evaluation of our approach on desktop and mobile devices.

• Jonathan Haberl, Philipp Fleck, and Clemens Arth are with Graz University of Technology. E-mail: jonathan.haberl@alumni.tugraz.at, {philipp.fleck | clemens.arth}@tugraz.at

Manuscript received xx xxx. 201x; accepted xx xxx. 201x. Date of Publication xx xxx. 201x; date of current version xx xxx. 201x. For information on obtaining reprints of this article, please send e-mail to: reprints@ieee.org. Digital Object Identifier: xx.xxx/TVCG.201x.xxxxxx

2 RELATED WORK

In this section we focus on the related work in 3DGS, which is relevant to our approach. Due to the vast amount of continuously published work, compiling a comprehensive overview is impossible. We also abstain from discussing the mathematical basics of 3DGS for brevity and refer the interested reader to the work of Kerbl *et al.* [14] for details. Because we introduce virtual memory to 3DGS in our work, we first briefly introduce the basics and then focus on related work required to understand the concepts. Thus, we bridge the gaps between 3DGS and virtual texturing.

2.1 3D Gaussian Splatting

In NVS, research is divided mainly into two state-of-the-art approaches: Neural Radiance Fields (NeRF) and 3DGS. While there are similarities, the latter was introduced by Kerbl *et al.* [14] to render radiance fields, representing scenes using an explicit scene representation. 3D Gaussians, stored as their ellipsoid equivalents, are defined by position, rotation, scale, opacity, and view-dependent color in the form of spherical harmonics. This representation allows them to produce accurate images that can be rendered in real-time on desktop hardware and edited easily. Images are rendered with a tiled software renderer implemented in Compute Unified Device Architecture (CUDA).

Taking inspiration from the initial proposal of 3DGS, researchers have explored a variety of further avenues and details, some of which are relevant to the concept proposed in this work.

2.1.1 Mesh Extraction

There are multiple reasons to create a triangle mesh from 3DGS scenes. The mesh may replace the scene representation entirely, or triangle meshes may support an application such as providing a foundation for physics interactions. The conventional method to extract a triangle mesh from a 3DGS reconstruction is to apply the Marching Cubes algorithm, proposed by Lorensen and Klein [21]. The algorithm converts 3D data to triangle meshes depicting constant-density surfaces.

Chen *et al.* [3] introduce a regularization term to 3DGS, encouraging thin Gaussians to better align with surfaces. Gaussians, as well as a neural network learning the scene’s Signed Distance Function (SDF), are jointly optimized to do this. Guédon *et al.* [9] introduce a similar regularization term. Waczyńska *et al.* [37] use a parameterization that defines Gaussians by their position on a mesh. Both the mesh and its Gaussians are optimized together. The idea of a joint representation for mesh and Gaussians is especially promising for deformation and has also been explored in that context by Yuan *et al.* [40] and Gao *et al.* [6].

We don’t aim to advance the field in this direction, rather we resort to using the Marching Cubes algorithm as a baseline for our work to also create a mesh for our purposes.

2.1.2 Compression

The concept of 3DGS implies the storage and handling of large amounts of data that increases significantly with the reconstruction scale. Kerbl *et al.* [14] use 248 bytes to represent a single Gaussian. The majority of this storage is consumed by the spherical harmonics that depict colors.

Pranckevičius [30] creates groups of Gaussians by their positions, whose properties he stores in patches in 2D textures. Morgenstern *et al.* [25] present an algorithm to efficiently sort millions of Gaussians by their properties in seconds to create 2D textures. Later, Pranckevičius [29] proposes using vector quantization with k-Means on spherical harmonics. Fan *et al.* [4] determine the importance of a Gaussian in a scene and use vector quantization on the less important Gaussians. Niedermayr *et al.* [28] determine the sensitivity of images to changes in properties to perform sensitivity-aware quantization. Vector quantization generates codebooks with an index to the respective entry for each Gaussian. Navaneet *et al.* [27] uses a form of Run-Length Encoding (RLE) on these indices, while Niedermayr *et al.* [28] compresses them with the DEFLATE algorithm, which also employs a variation of RLE.

Girish *et al.* [7] quantize Gaussian properties, then decode those with a Multi-layer Perceptron (MLP) to recover the initial properties. Li *et al.* [17] train an MLP to return a final color in dynamic scenes based on a base color, a view direction, and time. Lee *et al.* [16] determine a

feature and a view direction from positions with a hash grid and use those in an MLP to determine the color.

We do not employ any such compression in general, but our approach can be used alongside several of those extensions.

2.1.3 Large Scene Reconstruction

3DGS gains most of its popularity through its scalability to large scenes and the visual appeal of rendered imagery, albeit Kerbl *et al.* [15], complain about the lack of available huge datasets for further enhancements. Certainly, increasing the scale of reconstructions introduces a new range of challenges related to the amount of data that can be adequately stored in physical memory, making it essential to partition the reconstruction at some stage.

A dataset and an approach to partitioning large scenes is proposed by Lin *et al.* [18], splitting a scene into chunks based on the distribution of camera positions and the respective Structure from Motion (SfM) reconstruction. Liu *et al.* [20] split scenes into uniform chunks and prune chunks with low contribution to rendering. Kerbl *et al.* [15] define a low-resolution skybox on a sphere surrounding each chunk, defining the surrounding scene as background. Zhao *et al.* [41] follows a different approach, distributing Gaussians across multiple GPUs, assigning pixels to be rendered to GPUs in tiles and transferring the Gaussians between them as needed. Dynamic load balancing can make distributed training efficient and scale to up to 32 GPUs.

Both Liu *et al.* [20] and Kerbl *et al.* [15] make their code for scene reconstruction available. However, the scenes created by Liu *et al.* [20] are not available, and Kerbl *et al.* [15] introduce a new file format to incorporate their LOD implementation. We use a selection of the scenes from Lin *et al.* [18] for evaluation in Section 5. However, because of the differences in formats, direct comparisons to other implementations are generally challenging.

2.1.4 Streaming

In their initial work, Kerbl *et al.* [14], only perform frustum culling during rendering. A tiled, compute-based software rasterizer determines whether a Gaussian overlaps with a tile before sorting Gaussians for each tile individually. To do this, the data for Gaussians need to be in GPU memory. Jiang *et al.* [13] divide a scene into voxels. They determine which voxels lie in the view frustum using a KD-Tree and subsequently transfer these to the GPU. Kerbl *et al.* [15] asynchronously transfer high-detail Gaussians to replace those with lower detail as part of their LOD solution.

The use of streaming, or on-demand transfers, is still somewhat limited in current research. If it is used, the decisions for which Gaussians to copy is generally made based on the view-frustum, instead of any more sophisticated visibility determinations. In contrast, we perform visibility determination using a visibility buffer. Culling based on both the view frustum and occlusions are the result.

2.1.5 Level of Detail

Reducing the overall number of Gaussians to be rendered can significantly boost performance, while the most common approach is to merge multiple Gaussians. Yan *et al.* [39] propose combining Gaussians to solve aliasing problems in 3DGS. Gaussians that are too small during rendering are culled and replaced with larger ones. Kerbl *et al.* [15] introduce a hierarchy of Gaussians, merging them based on the contribution of each one on its parent. Their hierarchy allows them to choose which layer and therefore LOD level to render at runtime.

Liu *et al.* [20] do not reduce the number of Gaussians but compress those further away from the camera. Vector quantization proposed by Fan *et al.* [4] reduces the visual fidelity of less important Gaussians. Lu *et al.* [22] create anchors in a scene, spawning neural Gaussians around each that can be dynamically adapted to the distance. Ren *et al.* [31] create an octree for a scene, where each level represents an LOD level, each containing anchors spawning additional neural Gaussians.

We base our LOD solution on Yan *et al.* [39]. However, unlike most of the described methods, we do not modify Gaussians during scene reconstruction.

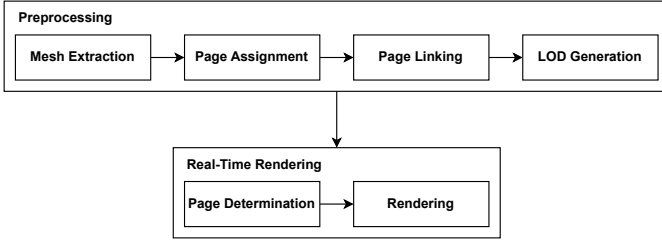


Fig. 2: Scene pre-processing and real-time rendering steps: A pre-processing stage prepares the scene offline. Real-time rendering steps are performed for every rendered frame.

2.2 Virtual Texturing

Virtual texturing is based on virtual memory, which modern operating systems and CPU architectures implement. Virtual memory separates virtual and physical address spaces. Memory addresses used by a process in userspace do not hint at actual locations in system memory but must be translated first. These translations query a page table, which maps pages of addresses in virtual memory to respective regions in physical memory once a process uses them. These pages are in regions of equal size in memory. The same system is used in modern GPU architectures. Applications can create buffers or textures that are not bound to any physical memory initially. Regions of these can be manually bound once they are required. This functionality is exposed to applications through modern APIs as sparse residency (Vulkan) or reserved resources (Direct3D 12).

Barrett [1] demonstrates how the concept can be applied to texturing, splitting textures into tiles (pages) of equal size. These tiles are generally not resident in GPU memory if they are not visible. At runtime, the scene is first rendered with tile IDs only, and visible tiles are copied to the GPU if necessary. An indirection texture points to the physical tile containing the required page. Mayer [23] provides a detailed overview and analysis of virtual texturing methods.

Virtual texturing forms the foundation for our work. We use these ideas to determine which pages are visible and transfer them to the GPU if necessary. Similarly to how mipmapping is integrated into virtual texturing, we integrate an LOD solution, and apply both concepts to improve 3DGS.

3 PREPROCESSING FOR 3DGS USING VIRTUAL MEMORY

Our virtual memory solution, inspired by virtual texturing, creates a mesh to approximate the 3DGS scene. Gaussians in the scene are grouped into pages. Rendering the proxy mesh quickly identifies which Gaussian pages are visible to the camera. In Figure 2 we provide a visualization of the steps involved with the method, while this Section is concerned with the upper part only. The lower part of Figure 2 is discussed in Section 4.

3.1 Mesh Extraction

To render a scene proxy, we need a simplified mesh with fewer primitives for faster processing while maintaining enough faces to prevent page occlusion. We must avoid small holes from Gaussians to minimize unnecessary pages. Intersecting ellipsoids (3D Gaussians) with the image plane creates scene slices, similar to the medical imaging applications of the Marching Cubes algorithm. Alternatively, this data can be represented by a uniform grid of sample points, each potentially inside one or more ellipsoids. These sample points correspond to pixels in the rendered scene slices.

To find the intersection between a plane and an ellipsoid, we use Hartmann’s method [12]. We define a plane normal to the Z-axis, adjusting the Z-coordinate as we scan the scene. Using a view matrix, we reposition the plane $z = 0$. The plane is in Hessian Normal Form, with its normal vector $n = (0 \ 0 \ 1)^T$, pointing in the positive Z direction, and its distance from the origin $p = 0$. We apply the ellipsoid’s inverse transformations to simplify finding the intersection, resulting in a unit sphere at the origin. We adjust the plane by multiplying its normal

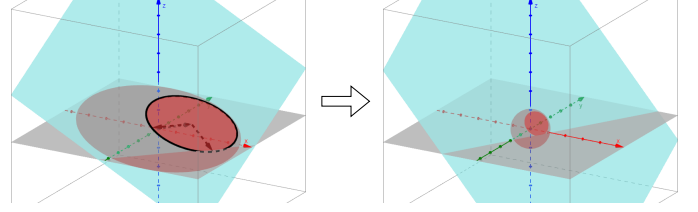


Fig. 3: The image depicts a red ellipsoid with its blue intersection plane, and the transformed unit sphere with the transformed plane on the right. When intersected with the image plane, ellipsoids form an ellipse (left). The ellipsoid is translated, rotated, and scaled into a unit sphere at the origin, with the plane adjusted accordingly (right). After determining the intersection circle, the original ellipse is recovered using inverse transformations.

vector by the Gaussian’s inverse rotation matrix and normalizing it, as shown in Figure 3. The distance from the origin is then determined by

$$p = \frac{v_z}{\|sn\|_2} \quad (1)$$

where v represents the ellipsoid’s translation in view space, and s its scale. A plane intersects the sphere if the origin is closer than the unit sphere’s radius, forming a circle centered at $c_0 = np$ with radius $r = \sqrt{1 - p^2}$.

$$c_1 = \begin{cases} \begin{pmatrix} p \\ 0 \\ 0 \end{pmatrix} & \text{if } n_z = 1 \\ \frac{p}{\|sn\|} \begin{pmatrix} (sn)_y \\ -(sn)_x \\ 0 \end{pmatrix} & \text{otherwise} \end{cases} \quad (2)$$

$$c_2 = \begin{cases} \begin{pmatrix} 0 \\ p \\ 0 \end{pmatrix} & \text{if } n_z = 1 \\ m \times c_1 & \text{otherwise} \end{cases} \quad (3)$$

We determine the parameters c_1 (Equation 2), and c_2 (Equation 3) to represent the circle as

$$c = c_0 + c_1 \cos t + c_2 \sin t, \quad (4)$$

which is subsequently transformed into an intersection ellipse using the Gaussian scale, rotation, and position, such that it can be drawn using its implicit representation.

Before applying Marching Cubes, we clean the data using morphological operations to close small holes and remove unnecessary detail, enhancing mesh simplification. These operations and kernels are tailored per scene for effective detail reduction. A surface is then reconstructed with Marching Cubes, and the mesh is simplified using a quadric error metric.

3.2 Page Assignment

To minimize the overhead of checking Gaussian visibility, we group them into pages. A proxy mesh face can correspond to none or multiple pages, while a page can cover multiple faces. Each page holds Gaussians up to a specified maximum. Initially, each mesh face gets a separate page, and Gaussians are assigned to the page of the face nearest to their mean. If a face gets more Gaussians than the page size allows, it is subdivided by adding a vertex at an edge’s midpoint, forming two triangles. This is repeated until each face has no more Gaussians than the target page size.

To prevent thin triangles from repeated subdivisions, we rotate the vertex order and choose different edges for subsequent subdivisions. The method isn’t optimal because shared edges may create vertices on adjacent triangles, leading to T-junctions and rendering artifacts due to floating point inaccuracies.

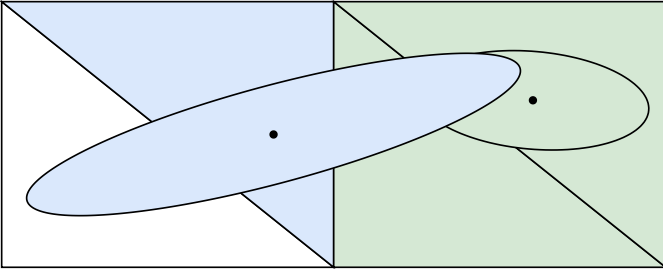


Fig. 4: 2D demonstration of a Gaussian, which has been assigned to a page based on its position, overlapping with another nearby page. Without page linking, the visibility determination for such a Gaussian may be incorrect.

Initial page assignments group nearby Gaussians but create small pages. We merge neighboring pages to approach the target size without exceeding it, using a greedy, breadth-first method. Pages are first merged with neighboring faces. If a page remains under the target size and no neighbors are left, a nearby page is chosen. If adding a page exceeds the target size, it becomes the base for a new merged page, to which more pages are added.

The initial pages, each per face, are greatly reduced. A triangular mesh face maps to one or no page, marked with a page ID for rendering if included. Unmarked faces lack a Gaussian mean match during initial assignment. Gaussians are grouped in memory once assigned to pages, with zero-property Gaussians added as padding to reach page size, easily culled during rendering.

3.3 Page Linking

In 3DGS scenes, millions of overlapping ellipsoids don't align with surfaces like textures do with mesh faces. We assign Gaussians to pages based on their means, without considering nearby interactions. Figure 4 shows how ellipsoids extending into surrounding pages can incorrectly be marked as invisible.

We address the issue by using page linking, identifying overlapping pages after initial assignment to establish uni- or bi-directional links. When a page is visible, all linked pages must also be present in GPU memory. To naively find pages that need linking, each ellipsoid is tested for intersections with others. Intersecting ellipsoids on different pages require links. Lacking acceleration structures, this approach has $O(n^2)$ time complexity, leading to trillions of tests even for small scenes. Instead, we generate random points within an ellipsoid and identify the nearest face on the proxy mesh for each. A link is needed if the face's page is different from the ellipsoid's assigned page. This approximate method tests only the closest face on the low-poly proxy mesh. This step is part of our algorithm for initial mesh assignment, allowing optimized page assignment and linking. Random points are generated uniformly in a unit sphere using spherical coordinates and converted to Cartesian coordinates. Applying Gaussian scale, rotation, and translation transforms these points to lie within an ellipsoid. The final distribution is non-uniform due to initial sampling in the unit sphere, not accounting for the ellipsoid's properties.

After assigning Gaussians to pages, a face on the proxy mesh may match one page. If the closest face for a sample belongs to a different page than its Gaussian, a link is established. If a mesh face isn't yet assigned to a page, it is marked with the page having the most sample points close to it. The page with the most overlap takes precedence, while other overlapping pages are linked. The number of page links indicates the quality of page assignments, which should aim to be compact and minimize overlaps. Future work may refine assignments based on these links.

3.4 Level of Detail

In mesh rendering, a mipmap is a texture with multiple precomputed, downscaled versions. As surfaces move further from the camera, lower resolution levels are used, improving performance by reducing texel fetches and offering anti-aliasing through bilinear filtering. Early virtual

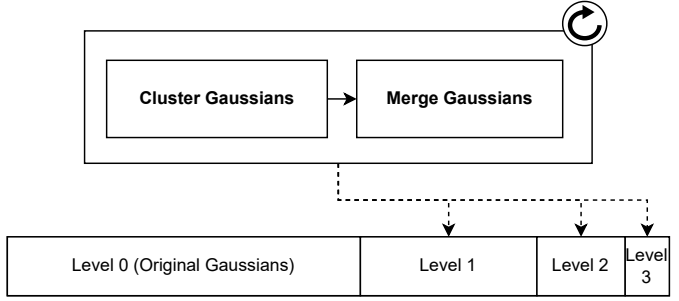


Fig. 5: Visualization of LOD generation for four total levels (including the original Gaussians as level zero). The number of Gaussians per page is halved for each subsequent level. Merging Gaussians is done with an average for all properties but their scale.

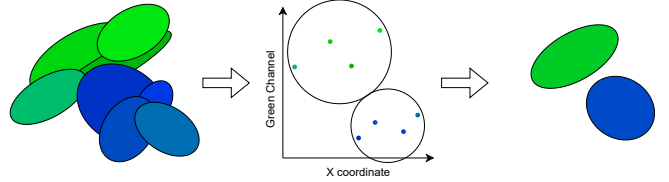


Fig. 6: Gaussians are clustered based on their properties, then averaged. This illustration clusters ellipses based on only their x coordinates and green channels. The ellipses are then averaged such that each cluster becomes one new ellipse.

texturing, like Mittring *et al.* [24], relies on mipmaps. The mip level is chosen when transferring a new texture to the GPU.

Mip level selection is performed based on derivatives. To calculate these derivatives, rendering is performed in groups of two by two pixels, known as quads. All pixels in such a quad are rendered for a primitive, even if the primitive only overlaps a single pixel. The pixels that do not overlap are helper pixels, executed in helper lanes, and are subsequently discarded. This can cause an overhead of up to three additional pixels per pixel rendered to the output image. LOD offers a solution with a mesh having various complexity levels, switchable based on camera distance, minimizing small primitives and reducing helper lanes, thus lessening performance impact.

Yan *et al.* [39] propose a method for 3DGS using mipmapping and LOD, merging Gaussians during training to create detail levels and reduce aliasing. We develop an LOD solution (Figure 5) based on this, but focus on minimizing the Gaussians to be copied, stored in GPU memory, sorted, and rendered, without altering the scene creation stage.

The objective is to merge Gaussians while minimally impacting their distant appearance. Only Gaussians on the same page can be merged. Their attributes are points in multi-dimensional space, making the task one of clustering these points by similar attributes such as position, rotation, and color. By scaling attributes, their influence on clustering is adjusted. Clusters are identified using the k-means algorithm. Figure 6 illustrates the concept by clustering and averaging ellipses based on two properties.

Merging multiple Gaussians is straightforward for most attributes using the arithmetic mean for translation, rotation, opacity, and spherical harmonics. However, as Yan *et al.* [39] note, merging scales can cause the resulting Gaussian to be too small. To remedy this, additional Gaussians are adjusted using average pixel coverage during training. We scale up the merged Gaussian by a fixed factor to fill gaps. In clustering, we prioritize position attributes to prevent dispersed clusters.

3.5 Scene Storage

The original 3DGS implementation exports generated data in Polygon File Format (PLY). Other applications, such as Nerfstudio [33], have followed suit. The data describing such a scene consists of a list of Gaussians with 62 properties each. The original encoding ensures quality despite numerical errors. Properties must be decoded from disk to display. Our virtual memory solution streams Gaussian to GPU

memory when needed, possibly loading just in time. Thus, we eliminate encoding and adjust the file format to stream data directly to the GPU. These modifications to the original format include:

- removing obsolete normal properties;
- reordering spherical harmonics data for better cache-locality;
- decoding the opacity property;
- decoding the scale properties;
- normalizing the quaternion describing the rotation.

We defer compression, such as converting spherical harmonics to half floats, to future work. Coordinate conversions, if needed, can be done by adjusting position, scale, and rotation. We limit the 3DGS scene to a central cube, excluding Gaussians with means outside it.

The mesh is stored alongside the modified scene file, including the following primitive attributes:

- a list of page IDs, with each entry corresponding to a mesh face;
- a buffer containing page links;
- metadata such as page size, number of LOD levels, etc.

4 REAL-TIME RENDERING

Rendering is time-sensitive. Modern applications require at least 60 Frames per Second (FPS), or frame times below a certain threshold, e.g. 16 ms. Virtual reality demands even higher rates to prevent nausea. Integrating rendering with other processes (e.g., physics simulations, pathfinding) can reduce the time available for each frame. Our real-time rendering concept allows for low-level optimizations. Parallelizable tasks are handled in thread pools or with compute shaders.

The proxy mesh loads instantly, but Gaussians use a memory-mapped file placed in virtual memory, with physical memory accessed on a page fault. Although physical access is slower and generally undesirable, this method allows 3DGS scene size to exceed system memory limits.

4.1 Page Determination

Before rendering a frame, we must determine which pages are visible from the camera. The aim is to cull Gaussians lying outside the view frustum and those occluded by other Gaussians. The Gaussians assigned to these visible pages must be copied if they are not yet in GPU memory.

For virtual texturing, Barrett [1] suggests rendering scenes with page IDs. All these IDs are needed for the final frame. We adopt this by marking our proxy mesh faces with page IDs, generating a list of visible pages from the image. Inspired by operating systems, we use a page table where each entry maps to a physical memory page, detailing virtual page properties. After listing required pages, new ones replace unused physical pages, prioritizing the least recently used. Once visible Gaussian pages are loaded into GPU memory to render the scene, we include the sorting of Gaussians by camera distance for alpha blending.

Page Links: We request pages via links, as explained in Section 3.3, where we preprocess scenes to identify overlapping pages. Each page’s visibility buffer includes its overlapping pages, and marking them as required minimizes visible artifacts.

Level of Detail: We add the distance of the nearest pixel to the visible pages list with its page ID. As the page table updates and new pages are copied, a suitable LOD is chosen based on this distance. This resembles choosing a mip level in virtual texturing. Barrett [1] segments mip levels into uniform-sized pages. We instead reduce Gaussians with each LOD, allowing multiple virtual pages within one physical page. We mark page table entries with their current LOD for this reason.

Thresholds, which can be dynamically updated based on memory usage, move away from the camera when usage exceeds a limit and move closer when memory is available. However, setting the initial threshold in fixed increments is problematic;

- If the step size is too large, a single step may affect memory usage drastically, overshooting the targeted region. This can lead to rapid flipping between two levels, causing noticeable artifacts.

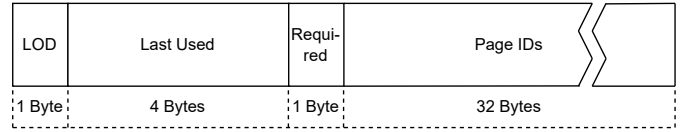


Fig. 7: Visualization of the page table entry for a single physical page. The entry contains the page’s current level of detail and the frame index for which the page was last required. For each virtual page within the physical page, a field indicates whether the page is required and the present page IDs.

- Differences in scene scale can make a step size too large, leading to the above mentioned issue, or too small, making the system slow to adapt.

Thus, the step size should be dynamically adjusted based on past moves to adapt plausibly.

4.1.1 Page Table Management

To track pages in GPU memory, we use a page table with entries describing the physical page contents, detail level, last use, necessity for the frame, and a detail-dependent list of contained pages. Figure 7 shows this page table entry. We selected a single array structure over a hierarchical one for better memory locality. The page table’s sequential iteration avoids field access indirection.

Page table updating involves two steps: First, it is traversed to update which physical pages are required based on the list of required page IDs. Free physical pages that is, pages that contain no valid page or pages that are not necessary for the current frame, are stored along with the frame in which they were last used. The list of required pages is simultaneously updated, removing pages already present in the page table at the correct LOD.

In stage two, the system checks the updated list of required pages, which contains page IDs to render the frame, none of which are in GPU memory. If there’s space, these pages are copied to a staging buffer, updating the page table. Free physical pages are chosen based on the least-recently-used order, then moved from the staging buffer to the Gaussian buffer on the GPU. We use a regular buffer, skipping the sparse residency feature described in Section 2, for three main reasons:

- In virtual texturing, textures are addressed using UV coordinates, typically needing translation via an indirection texture, adding a lookup overhead. We avoid this lookup and use an index buffer to indicate Gaussians for drawing, which must be sorted regardless of sparse buffers.
- Only a few newer high-end desktop GPUs support it. The hardware capability database [38] indicates that less than a third of GPUs permit the `sparseResidencyBuffer` feature. For Android devices, support is just over 10%. Without MoltenVK [36], bridging Vulkan and Metal, Apple devices generally lack this feature.
- Even on recent hardware with sparse residency, performance seems to be unsatisfactory as mentioned by Richermoz [32].

The list of physical pages is written to a buffer to indicate required pages to the renderer. The compute shader is adjusted to convert these pages into sortable indices based on camera distance.

4.2 Rendering

There are generally two approaches to rendering 3DGS scenes. Kerbl *et al.* [14] use CUDA to create a software renderer. The image is split into tiles, determining the Gaussians overlapping with each. Each tile’s Gaussians are sorted and then drawn to the output image. Our implementation instead opts to sort Gaussians globally in a OpenGL Shading Language (GLSL) compute shader before splatting the Gaussians onto quads rendered using the hardware rasterizer.

The quads can be constructed in multiple ways, as depicted in Figure 8. One option is to record and submit commands to draw point primitives. This dispatches a vertex shader for each Gaussian, performing the necessary calculations. If geometry shaders are available, a geometry shader constructs the quad by emitting four vertices in a

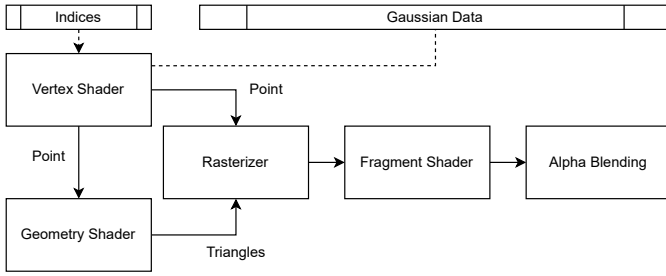


Fig. 8: Simplified overview of our pipeline used to render Gaussians. A vertex shader is supplied with a sorted index buffer, which it uses to retrieve properties for its respective Gaussian from a storage buffer. If the device is capable of a geometry stage, a geometry shader is used to construct a rectangular quad. Alternatively, a point primitive is used. A fragment shader draws an ellipse onto the quad. Finally, the quads are combined via alpha blending to create the final image.

triangle strip. Finally, a fragment shader discards pixels outside the splatted ellipsoid. If geometry shaders are unavailable, however, we can fall back to a pipeline, omitting the geometry stage. The quads are then the result of the point primitives, passed to the rasterizer. Their square shape can lead to a significant increase in fragment shader invocations, leading to discards. In Figure 9 three extreme cases are explored. The area shaded red indicates discards that are avoided with a geometry shader. In the middle case, the number of discards remain the same. On hardware that supports it, even a mesh shader pipeline may be preferable to generate quads to avoid the performance penalty of enabling geometry shaders. However, we did not consider this aspect in our work.

Gaussians with opacity require alpha blending and must be sorted by distance to the camera. The rendering order is determined by constructing and globally sorting an index buffer with one index per Gaussian. Compute shaders handle this process: one calculates distances from the camera, another uses a radix sort to reorder indices, and finally, indices are sent to the vertex shader to access attributes from a storage buffer.

The math for drawing each Gaussian remains substantially the same from Kerbl *et al.* [14]. The majority of the required calculations, described in Section 3, are performed once per Gaussian. They can, therefore, be performed in the vertex shader. The fragment shader is then responsible for shading the projected Gaussian within a quad based on a 2D covariance matrix.

4.3 Limitations

Our rendering concept has deficiencies that need addressing to scale to even larger scenes or enhance performance. These issues may overlap with those discussed in Section 3 and will be detailed later. However, the most conceptual issues are discussed in the following.

After rendering the proxy mesh image, it is reduced to a buffer indicating each page’s visibility. Hable [11] discusses the performance impact of `gl_PrimitiveID` and suggests using the leading vertex to determine triangle primitive IDs. A compute shader reduces the visibility buffer to a list of IDs. To communicate additional LOD levels, the distance to the closest pixel is stored. Since finding this minimum can lead to race conditions, atomic operations are employed, impacting performance with concurrent thread updates. To enhance performance, it’s better to minimize atomic operations, especially in global memory, and use faster shared memory within workgroups before accessing global memory. We mitigate these shortcomings by rendering the visibility buffer at low resolution, which can cause distant pages to be missed. Mayer [23] demonstrates how smaller visibility buffers improve performance with virtual texturing. However, unlike virtual texturing, overlapping Gaussians cause nearby pages to remain memory-bound.

Our page table is a single array of entries, each managing a physical page, which may include multiple pages depending on the LOD level. We avoid hierarchical page tables found in operating systems to reduce indirections and potential page misses. Further work is needed to shrink page entries and test scalability with buffer size for rendering.

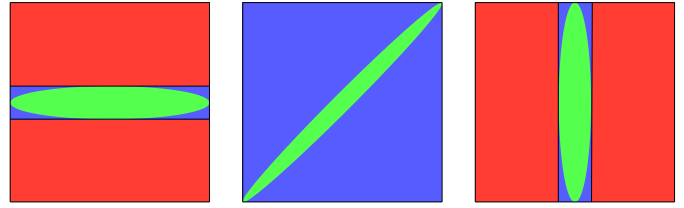


Fig. 9: The area resulting in discarded pixels when drawing a long, thin ellipse. A point primitive is always square, resulting in fragment shader invocations that lead to a discard for pixels in the red and blue areas. Only the blue area is discarded when using a geometry shader to fit the quad more tightly to the ellipse. In the second image, the rotation of the ellipse causes any advantages to be lost, the overdraw is the same with and without a geometry shader.

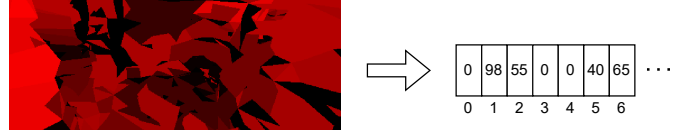


Fig. 10: Rendered primitives are shaded based on the ID of their page. The buffer inside the compute shader holds one entry per page. The entry indicates that a page is visible by setting its respective entry to a value other than zero. Values encode depth for LOD level selection.

The page table entries, among other parts of the system, would also require modification to allow blending between LOD levels. During the transition, both levels are needed in memory simultaneously.

Both LOD transitions and adding linked pages are less urgent than rendering visible Gaussian pages. The copy budget is limited by the staging buffer size and the time required. To maintain quality under high load, we prioritize important copies and delay LOD transitions to later frames.

Strict synchronization during frame rendering causes pipeline stalls. The GPU could do more work but waits for task completion. Efforts to separate steps and perform tasks asynchronously could speed up rendering, especially data copying from CPU to GPU.

Mobile devices, including those by Apple, generally contain integrated GPUs nowadays. Memory is shared between CPU and GPU. To take advantage of this properly, modifying our concept could avoid streaming any data overall. Instead, memory could be mapped from the file directly to the buffer used by the GPU to render Gaussians. Finally, Gaussians are rendered using the GPU hardware rasterizer. Kerbl *et al.* [14] uses a software renderer in CUDA, breaking cross-platform portability in turn. Our concept neglects CUDA and is less restrictive. Nevertheless, the leverage of compute shaders for the proposed concepts could be advantageous on one or the other hardware.

5 EVALUATION

This section evaluates the method and implementation described in this work. In particular, we explore our results regarding visuals, memory use, and performance.

5.1 Details on Prototypical Implementation

To better understand the visualization, we initially present important insight to our Vulkan-based implementation. The interested reader is referred to Haberl [10] for a more in-depth description.

5.1.1 Page determination details

We render the proxy mesh to a visibility buffer using a single-channel 32-bit unsigned integer image. This image can be much smaller than the final rendering while still delivering effective results. Page linking enhances this by connecting nearby pages, minimizing the effects of a smaller rendered image.

The vertex shader receives vertex positions and applies model and camera transformations used later in the scene. The fragment shader gets a buffer of page IDs for each face, with the input variable supplying

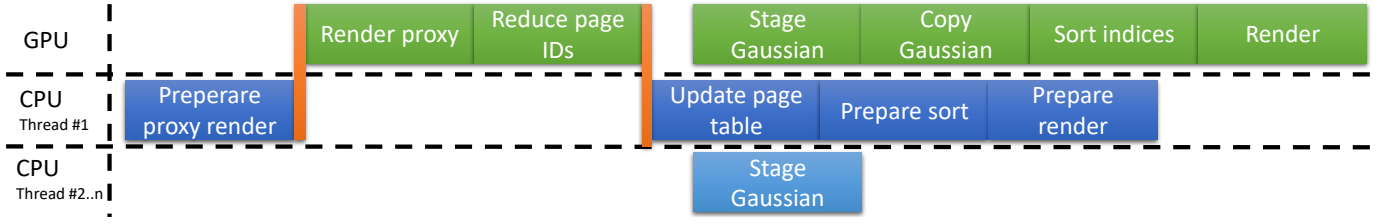


Fig. 11: High-level overview of the stages of rendering with virtual memory. Orange bars indicate synchronization between CPU and GPU. Each step additionally depends on the previous step in the same lane. The tasks are not scaled with the time it takes to complete them.

the face index to output the corresponding page ID. Background and unassigned faces result in a zero page, ignored in later steps.

After rendering the proxy mesh, we reduce the data by creating a buffer indicating required pages. A compute shader updates each pixel’s list entry in parallel, encoding depth as integers that decrease with greater depth. Using the `atomicMax()` function, only the closest depth value is written to the buffer. We iterate through linked pages per pixel to set buffer entries. Once transferred to CPU memory, the array shows zeroes for unneeded and depth values for needed pages. Selection is based on depth value LOD, as visualized in Figure 10. Transitions between detail levels are adjusted at runtime based on used to free memory ratio, aiming for 50-80% usage. Thresholds are moved if outside this range, increasing step size by 1% after successive similar adjustments or decreasing it by 1% if direction changes quickly.

5.1.2 Transfer

The buffer of Gaussians is memory-mapped on the CPU, enabling buffer access while file reads are managed by the OS. Discrete GPUs’ large memory segments are not directly accessible from the CPU. We copy these to host-visible memory for writing, despite its small size and slower GPU access. This staging buffer is vital for discrete GPUs, as they have independent memory separate from the CPU, connected typically via Peripheral Component Interconnect Express (PCIe). Integrated GPUs, used in mobile devices, share memory with the CPU, making all accessible memory host-visible but with lower throughput. The implementation completes all memory transfers before further steps, with potential enhancements through separate GPU queues for reduced framerate impact.

5.1.3 Synchronisation

Work is largely performed on the GPU. Steps in Figure 11 benefit from parallel execution but require synchronization. The page update begins with recording commands to draw the proxy mesh and reduce page IDs, separated by a pipeline barrier to ensure memory is flushed before processing results. These commands are submitted to a graphics and compute-capable queue. We use a fence to wait before updating the page table on the CPU. Data transfer to the staging buffer starts during the page table update, with multi-threaded transfers handled by the drivers. After updating, Gaussians are copied to the second command buffer, also containing depth sorting and drawing, separated by a barrier. Commands are recorded during data transfer in separate threads. Depth sorting via compute shaders requires nine dispatches with metadata in a uniform buffer, defined by a push constant. Lean barriers prevent pipeline stalls. Post-dispatch, depth results move to the index buffer. Rendering the final 3DGS scene uses the updated index buffer. After updating the page table and completing transfers, command buffer submission triggers a semaphore, presenting the image. Two frames can be processed simultaneously, with work on the CPU while the GPU presents the previous frame.

5.1.4 Adaptations for Mobiles

We port our real-time renderer to iOS to test its viability on mobile devices. Since Apple prefers the Metal API over Vulkan, we use MoltenVK from the Khronos Vulkan Portability Initiative [8] to bridge Vulkan and Metal, allowing our existing Vulkan code to run on macOS and iOS. Despite some extension support differences with Windows, the essential extensions required are supported. The main differences

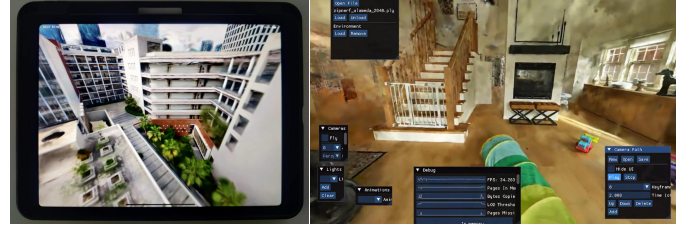


Fig. 12: Our implementation running on an iPad Pro. The application is not specifically optimized for mobile devices with integrated GPUs. It uses the same Vulkan code for rendering with MoltenVK as a translation layer to the Metal API.

between desktop OS (Windows, macOS) and iOS relate to file handling. An iOS app bundle includes an executable and resources, while it can read from and write to an app-specific, sandboxed directory. We package all shaders and test scenes into the app bundle, using the POSIX function `mmap(...)` for memory mapping. Apple devices fully support POSIX, and system interactions are feasible via the C++ standard library. While we adjust Vulkan and file-related code to ensure our implementation compiles and runs, we do not optimize for mobile devices or iOS specifically. Figure 12 shows the application on a 3rd Generation iPad Pro.

5.1.5 Build Details and Test Hardware

As mentioned, our renderer is implemented in C++ using Vulkan, which uses the hardware rasterizer. The evaluation is done on Windows computer and we compile our application with Microsoft Visual C++ (MSVC). The build type is set to `RelWithDebInfo` to optimize the binary for best performance. We disable any Vulkan validation layers during our evaluation.

Our testing hardware includes an NVIDIA GeForce GTX 1070 GPU and Intel Core i7-4770k CPU, using Double Data Rate 3.0 (DDR3) system memory to transfer Gaussian via PCIe 3.0. Though not state of the art, this setup is expected to remain common among consumers [34]. Thus, good performance on such devices is crucial for 3DGS’s adoption. We also test our method on an Apple iPad Pro, model A2377 with an Apple M1 System-On-Chip (SoC), featuring CPU and integrated GPU, to assess performance impacts on mobile devices and guide future development regarding integrated GPUs.

5.2 Qualitative Analysis

We evaluate various 3DGS scenes of different sizes, defining a camera path for each using a perspective camera with a 90° Field Of View (FoV). The camera moves at a fixed speed, interpolating its position and orientation between checkpoints. Paths are designed to encompass diverse scenarios, including close-ups and distant overviews, thoroughly navigating the scene to engage multiple Gaussian pages at varying detail levels, thereby showcasing the method’s strengths and weaknesses.

As the camera follows its path, we track key statistics per frame: memory used by active Gaussians, and the time to render the proxy mesh, list pages, update the page table, copy data, sort, and render Gaussians.

Large scenes are expected to make extensive use of LOD, while complex scenes with potential for occlusions allow us to eliminate many Gaussians from rendering. We therefore choose a selection of

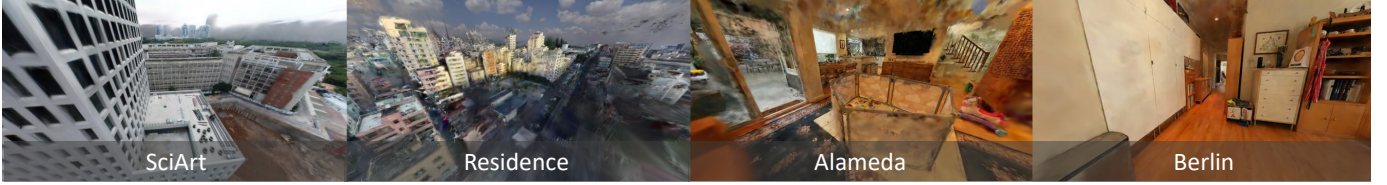


Fig. 13: Example images of the evaluated scenes: *SciArt* and *Residence* are taken from the UrbanScene3D [19] dataset and trained with VastGaussian [18]. And *Alameda* and *Berlin* are from Zip-NeRF [2] and trained with Nerfstudio [33].

Scene	Initial Size [MiB]	Pages	Links	File Size [MiB]	Pre processing [s]
SciArt	804.9	3778	49576	1505.5	2600
Residence	2214.6	4954	65856	4281.5	4579
Alameda	353.9	730	10664	630.9	1169
Berlin	236.5	492	6444	425.2	921

Table 1: Evaluation statistics for scenes with a page size of 2048 include initial sizes post-reconstruction, followed by updates such as padding and added LOD levels, affecting final sizes. Preprocessing times for each scene are also provided.

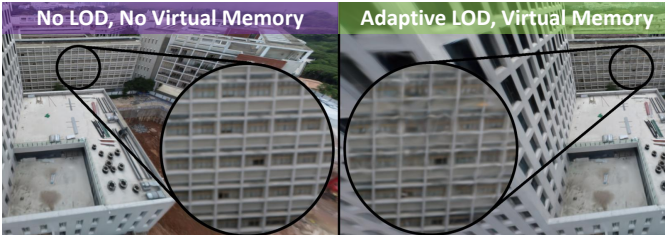


Fig. 14: Similar quality, smaller memory footprint: To avoid creating holes due to lack of available memory, the scene is rendered entirely without virtual memory. Virtual memory with adaptive LOD is enabled. Close to the camera, the original Gaussians are rendered.

large-scale scenes trained with the methods introduced by Lin *et al.* [18]. Kerbl *et al.* [15] present a similar dataset in their work on large-scale rendering, but it is not available at the time of writing. Smaller scenes with obstructions are created from images by Barron *et al.* [2] and trained using Nerfstudio [33]. The selected scenes are listed in Table 1, with an image of each in Figure 13. Datasets in novel view synthesis often consist of images of a single central object captured from all angles. They contain negligible amounts of occlusion and, therefore, generally do not benefit significantly from virtual memory. We omit testing for these types of scenes.

Table 1 presents statistics per scene with a 2048 page size. Page numbers correlate with Gaussian counts despite padding. Adaptive LOD allows the same buffer for scenes with varying pages, aiming to maintain stable frame times and memory. When pages exceed the buffer, higher LOD levels decrease quality. Alternatively, positioning the camera to capture fewer pages permits rendering at lower LOD levels, improving results. Creating a 3DGS scene involves steps like SfM, training, and preprocessing, which are not deterministic and may lead to different statistics on recreation. We consistently find an average of 13-15 links per page across scenes. Similar to mipmaps, halving the page size with each LOD level nearly doubles the final size. The overhead we introduce is negligible compared to the size of the original scene. We store the proxy mesh with its page IDs, metadata, and page links in a single file. This file stays below 20 MiB in all listed scenes.

Preprocessing times excluding slice rendering are given in the last column in Table 1. Factors like size, scene structure, and hardware impact these times. The largest scene, residence, requires over an hour to preprocess, with 85% spent on LOD generation. Its structure makes k-means converge slowly. For most scenes, page assignment, linking, and LOD generation each make up half the preprocessing time. Excluding residence, each page adds about half a second. LOD generation, being highly parallel, can be accelerated by reducing iterations or using a faster CPU with more cores.

ArtSci	PSNR [dB]	SSIM
With page links, with LOD	42.89	0.99
Without page links, with LOD	35.02	0.97
With page links, without LOD	47.19	0.99
Without page links, without LOD	35.02	0.97

Table 2: Comparison between images rendered without virtual memory and with ablations of our virtual memory solution.

Page assignment is solely position-based. Gaussians at the building’s top, likely facing upward, should be rendered even if they’re not in the visibility buffer. With page links, pages at the front and top are linked due to overlap. Figure 14 contrasts scene rendering without virtual memory against using it with LOD. Gaussians further from the camera use higher LOD levels. During preprocessing, Gaussians within a page are combined to halve those of the lower level. At runtime, memory use determines the distance from the camera where LOD level changes. Higher levels are applied further away, slightly lowering visual quality, but clustering such pages in a render buffer boosts performance.

The preprocessed scene is loaded to prepare for real-time rendering. The scene is rendered using virtual memory with the implementation described in this work. To determine their impact, we enable the methods presented separately (linking, LOD, etc.). In Table 2 we calculate Peak Signal-to-Noise Ratio (PSNR) and Structural Similarity Index Measure (SSIM) between an image rendered with and without virtual memory. We render the same image with various ablations of our method. Figure 15 contains all image variations and their differences from the scene rendered without virtual memory. None of the configurations are memory-constrained; all required pages fit in memory.

When LOD is disabled but page links are used, almost all of the 500 available pages are used. With buffer usage above 80%, adaptive LOD reduces the distances for level transitions. Image quality suffers as a result, with a sharp drop in PSNR. With our test setup the ranges adaptive LOD lands on to satisfy conditions on memory use are not deterministic. When page links are not used, noticeable artifacts appear in the image which is reflected in the image comparison scores. These scores listed in Table 2, as well as the right image in Figure 15, indicate the best quality with page links enabled and LOD disabled. This makes sense given that page links increase the number of required pages to produce better results while LOD diminishes quality to regain memory. However, this quality can only be achieved because all required pages, even with the additional pages requested due to page links, can fit into the 500 page buffer. If this were not the case, additional artifacts would be introduced. Disabling page linking (Figure 15 (b) and (d)) leads to the expected artifacts explored previously. Enabling both methods can be thought of as balancing quality and memory usage. In Figure 15, there are little to no differences for parts of the scene close to the camera. Page links fulfill their part of contributing pages not visible on the proxy mesh but overlapping with pages that are. Simultaneously, when those pages are distant, a different LOD level is used, which reduces quality slightly.

Limitations Figure 16 demonstrates the issues our current page link method presents. No special care is taken to avoid reducing the number of page overlaps during preprocessing. In extreme cases, this can negate the occlusion culling effect achieved by the visibility buffer entirely. While LOD might mitigate overhead, higher LOD levels may lower quality. LOD lowers Gaussian page quality, with artifacts appearing when merging over distances. Though minor when far from the camera, these artifacts become significant near the camera at high LOD levels,

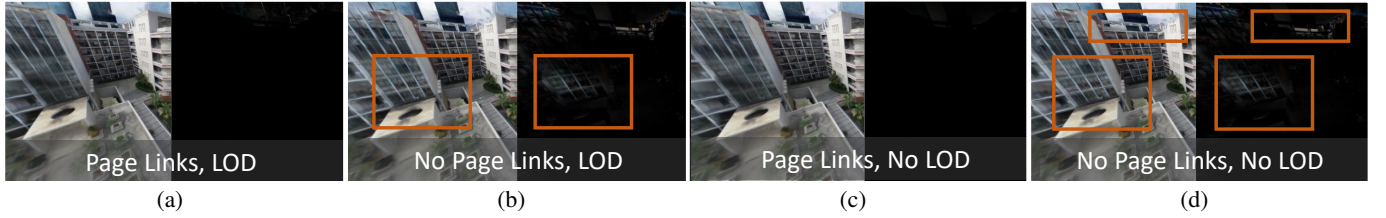


Fig. 15: Images with the same camera position and settings, rendered with ablations of our method (left). Images on the right compare these to the same scene rendered virtual memory. Black indicates no difference, pixel brightness indicates how large the difference is.

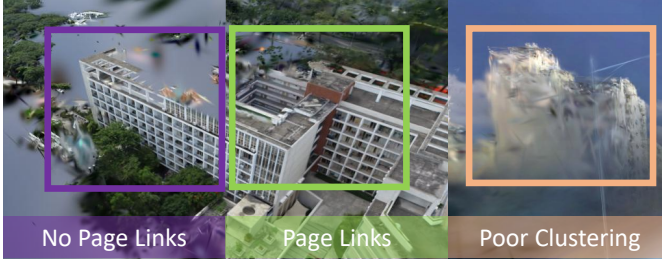


Fig. 16: No Page Links leading only the pages of Gaussians determined to be visible based on the visibility buffer are transferred and rendered. Enabled page links, causing significantly more pages to be rendered based on page overlaps. Poor clustering of Gaussians to merge can create artifacts, which becomes obvious when high LOD levels are used close to the camera.

Page Size	Page Table Update [ms]	Depth Sort [ms]	Render [ms]
2048	0.9	2.0	8.0
4096	0.5	3.0	9.7
8192	0.3	6.7	10.6

Table 3: Comparison of median time taken for selected rendering stages with different page sizes. In all tests, the camera follows the same predefined path. As the page size increases, page table updates shorten, while depth sorting and rendering take longer.

as shown in Figure 16. Reducing page overlaps and adjusting Gaussian scales can decrease artifacts. Our method does not blend levels to hide popping during LOD level transitions, a feature left for future versions with 3DGS’s alpha blending capability.

5.3 Quantitative Analysis

Grouping Gaussians together enhances cache locality, increasing cache hits during rendering, especially with virtual memory. Although page order doesn’t reflect Gaussian proximity, streaming visible pages to a smaller buffer brings pages closer. Larger page sizes raise position variance and cause more Gaussians to be falsely marked visible due to a less atomic visibility buffer, while smaller sizes add overhead to page table management and memory transfers. Table 3 compares timings of selected rendering stages for different page sizes. Other stages are largely unaffected. Notably, the time gained updating the page table at larger page sizes does not seem to outweigh the penalty of unnecessary Gaussians and reduced cache locality, at least for large scenes. To reduce the impact of cache locality, future implementations may additionally choose to reorder Gaussians within each page based on the Morton order. Table 3 indicates, that a 2048 page size is appropriate to balance cache locality with page table management overhead. The size of the staging and rendering buffers is crucial. A larger staging buffer permits longer delays, as copying Gaussians blocks depth-sorting and rendering. Conversely, if the buffer is too small for all required pages yet fails to present pages in GPU, artifacts like holes and popping occur. Our staging buffer is set to a size of $\sim 18.4\text{MiB}$, equal to 40 pages of 2048 Gaussians.

The rendering buffer size significantly affects performance. The buffer must be large enough to hold visible pages. LOD addresses performance issues from rendering numerous Gaussians: **Our implementation adjusts LOD levels based on memory usage. In other**

Buffer Size [Pages]	Without LOD		With LOD	
	Render [ms]	Missing Pages	Render [ms]	Missing Pages
250	3.8	549	5.0	0
500	6.6	263	6.7	0
1000	8.1	0	8.4	0

Table 4: Comparison of median render times and number of missing pages for different buffer sizes with and without LOD. Buffer sizes are specified as a multiple of the page size. Both with and without LOD, the render time increases with the buffer size. However, LOD reduces the necessary memory to contain the required pages.

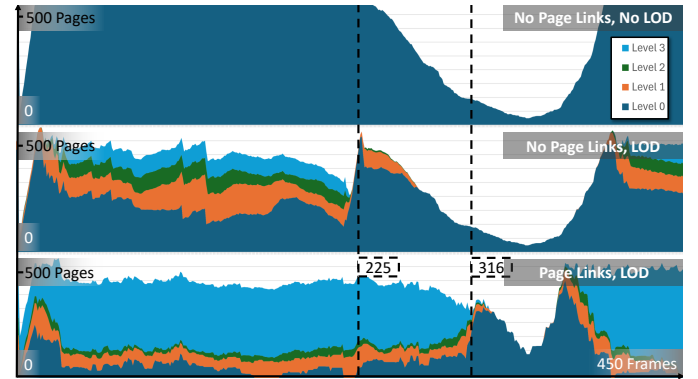


Fig. 17: Memory usage during a fly-through in the scene “Residence” with different ablations. This scene contains almost 5000 pages of Gaussians with the first LOD level taking up more than 2 GiB. With a 500 page buffer only $\sim 10\%$ of Gaussians can be rendered at a time.

words, it aims to fit all required pages into the buffer to avoid holes. As a side effect, large buffers allow many Gaussians to be rendered at low LOD levels (more details), negatively impacting performance. Table 4 examines the link between buffer size, render times, and missing pages. Without LOD, smaller buffer sizes are too small to hold all visible pages. As a result, render times increase when increasing the buffer size. When using adaptive LOD, distances are chosen to avoid any holes due to missing pages. **As a result, a smaller buffer can render the same scene without artifacts.**

5.3.1 Memory Usage

We assess memory usage for two scenes in more detail. The camera follows a path through each, with different ablations. As the camera moves, the number of rendered pages changes. In Residence (Figure 17), a large open scene, memory is quickly saturated without LOD enabled. In contrast, Alameda (Figure 18), which features many occlusions but is limited in size, memory use never exceeds 50%.

Upon enabling LOD, memory use in Residence is reduced drastically. A single physical page can store up to 2, 4, or 8 pages, respectively, at higher levels. Adaptive LOD attempts to keep memory use between 50% and 80% and modifies the distances at which levels transition to achieve this. Alameda, which uses limited memory, is not affected by enabling LOD. All required pages fit within the 80% limit in memory at all times, resulting in the use of level zero throughout.

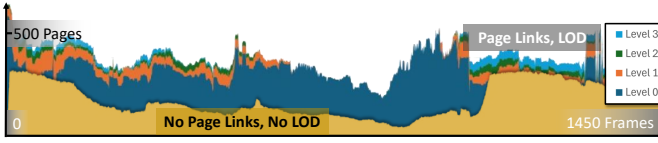


Fig. 18: Memory usage during a fly-through in the scene "Alameda" with different ablations. This indoor scene contains many occlusions but only 730 pages in all.

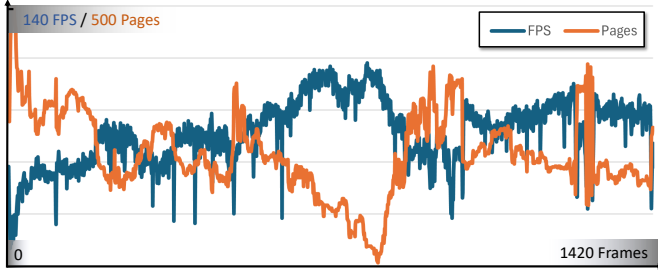


Fig. 19: FPS observed along a fixed camera path, compared to the number of rendered pages. FPS are not smoothed; they are determined by the time between subsequent frames. Performance clearly correlates with the number of Gaussians rendered. Frame times decrease as the number of pages decreases.

When page links are used, memory usage is increased drastically. A large number of physical pages are populated with level three pages in Figure 17. This indicates adaptive LOD needs to set the distances for level transitions close to the camera in order to keep memory use within the targeted range. A similar increase in rendered pages can be observed in Figure 18, where multiple levels of detail are now required.

Page linking can indeed degrade image quality by increasing memory needs, leading to poorer rendering LOD. However, without page links scenes may show artifacts, as seen in Figure 16. As a tradeoff, careful page assignments and setting a threshold to ignore small overlaps can minimize page links without causing significant artifacts. Overall, using virtual memory significantly reduces memory usage and the count of Gaussians rendered. Without virtual memory, full scenes equate to 4417 and 724 pages. In the "Alameda" scene, visible Gaussians are at most 35% of the total due to occlusions.

5.3.2 Performance

Performance, measured in FPS, is closely correlated with the number of Gaussians rendered (Figure 19). As the number of pages increases, the FPS drop. This is indicative of the effectiveness of reducing the number of rendered Gaussians to improve performance. In the following we discuss selected frames from the Berlin scene with a certain impact:

- **Most Pages.** One of the frames with the highest number of physical pages in active use.
- **Median.** The median time taken to complete each step over the entire path. This is not a real frame but rather a reconstruction meant to approximate the median frame.
- **Shortest.** The frame with the smallest sum of the time taken by each step.
- **Largest Transfer.** The frame with the most bytes of Gaussian data copied to GPU memory.

Rendering the visibility buffer and reducing it to a list of page IDs takes an almost constant amount of time. Page table updates are nearly constant, with a slight delay when adding many new pages. Most frames have no waiting overhead for the staging buffer copy. For the frame with the largest transfer, this is a minor issue. Sorting by depth and rendering time scale with the number of Gaussians, with rendering time being crucial to minimize.

The effectiveness of virtual memory can be seen when rendering the scene without virtual memory and comparing the timings (Figure 20).

GPU	FP32 [TFLOPS]	Bandwidth [GB/s]
NVIDIA GTX 1070	6.5 [35]	256.3 [35]
Apple M1 SoC	2.6 [26]	68.3 [5]

Table 5: Basic comparison of the iPad Pro's integrated M1 GPU to the dedicated GPU used for evaluation on desktop. FP32 measures the number of 32-bit floating point operations per second (in trillions).

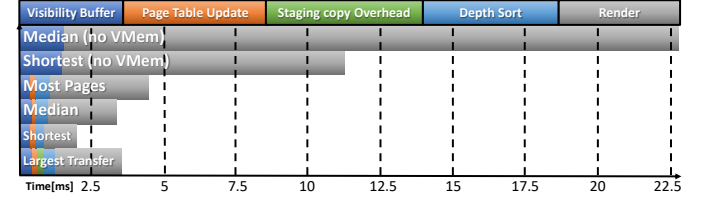


Fig. 20: The time taken for various steps with virtual memory as well as the median and shortest frame rendered without virtual memory. The overhead associated with virtual memory is negligible when compared to the time gain for depth sort and render stages.

The chart contains the timings shown in Figure 21 but adds additional data without the use of virtual memory. The rendered scene contains the same Gaussians as the base level of Gaussians with virtual memory. Gaussians are not grouped into pages, reordered, or padded. Therefore, it does not benefit from visibility determination or improved memory locality.

Rendering the Berlin scene uses 489 pages in virtual memory, fitting comfortably in a 500-page buffer. Excluding hidden pages notably improves frame times. Frames without virtual memory take longer than previously analyzed ones, with the median frame taking even more time. Without virtual memory, page management overhead is eliminated. Timing shows the benefits of these preparatory steps, as even the depth sort stage is quicker. Rendering speeds up significantly due to improved memory locality and fewer Gaussians to process.

5.3.3 Mobile

Our concept renders discrete and integrated GPUs identically under the same configuration and swapchain image size. However, based on Table 5, performance varies across devices. The iPad's M1 is a SoC with CPU and GPU on a single chip, sharing the same memory. Vulkan reports just a single memory heap where memory may be accessed by both device and host. Our application makes no use of this, instead keeping the same data in memory multiple times. In an optimization file backed memory can be used by the GPU directly and no manual streaming is necessary. After measuring timings we can therefore make some limited assumptions about performance without streaming.

With the same configuration and camera paths, only performance varies between desktop and mobile. Initially, comparing baseline performance without virtual memory, Figure 22 shows frames take longer on mobile due to a fourfold increase in Gaussians sorting time, indicating slower memory access as expected with an integrated GPU. Enabling virtual memory reduces the Gaussians needing sorting. This method's overhead is justified, as depth sorting and rendering are significantly faster. However, mobile's virtual memory time is still much higher than desktop's, a gap a software renderer could likely reduce.

Figure 23 shows mobile-measured times for a larger scene with frame times over 200 ms without virtual memory. Our method reduces time by culling Gaussians, though streaming overhead remains due to slow memory access and lack of optimization for integrated GPUs. We simulate median times without streaming overhead, potentially possible with file-backed memory. However, even then, it's not interactive. Large scenes need further optimization like reducing buffer sizes or software rendering.

Overall, performance on mobile is mainly impacted by memory accesses. This is especially noticeable during our global depth sort. Our virtual memory method, apart from the unoptimized streaming, is not greatly impacted by the move to mobile.

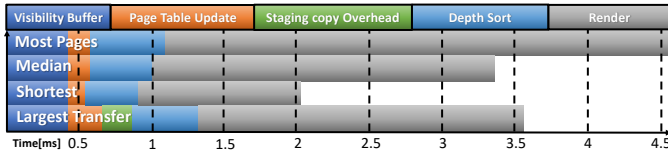


Fig. 21: Comparison of the time taken for various steps when rendering a frame with virtual memory. Specific frames are selected for further analysis. The median frame is not an actual frame but a combination of the median time taken by each step.

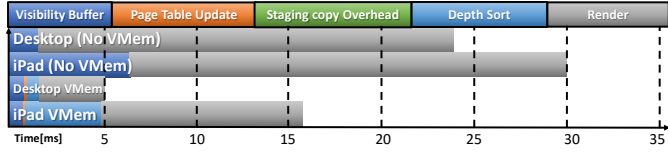


Fig. 22: Comparison of the time taken to render frames on desktop and mobile. All frames are a collection of the median times for each stage along a path. The first two bars are a baseline, without virtual memory enabled.

5.4 Discussion

Our initial assumption is that the number of rendered Gaussians directly affects performance. For an approach to be effective, an induced reduction in render time must exceed the overhead of identifying visible Gaussians. This is clearly confirmed by our results. We expect this to also hold true with different rendering approaches, including the software renderer from Kerbl *et al.* [14].

Our proxy mesh strategy effectively reduces memory in large scenes and relies on acceleration structures for fast Gaussian determination, as mentioned in Section 2. However, unlike other methods, it handles occlusions well, boosting performance in occluded environments such as indoor and city street-level datasets. Our approach also allows virtually unlimited scene size during rendering at a reasonable scale and speed.

Published datasets and implementations for large-scale scenes are inadequate. Common 3DGS training implementations poorly handle occlusions, creating artifacts. Datasets often originate from Unmanned Aerial Vehicle (UAV)s with few occlusions. The dataset from Kerbl *et al.* [15] is promising but uses a non-standard file format.

Gaussians can't map directly to surface textures, so we use page links, which help avoid rendering artifacts but increase memory usage. We plan to enhance link creation to use fewer pages. LOD integrates with our solution like mipmapping with virtual texturing, crucial for maintaining a strict memory budget without significant quality loss. Our LOD system has flaws in creation (incorrect scale) and rendering (lack of level blending). Integrating recent works from Section 2 can address these issues.

6 CONCLUSION AND FUTURE WORK

In this work, we demonstrate the viability of applying the concepts used in virtual texturing to cutting-edge research in 3DGS. A proxy mesh is generated from an existing 3DGS scene, grouping Gaussians into pages with IDs and linking them if overlapping, forming several LOD levels. Rendering this mesh to a visibility buffer enables fast visibility checks. Pages are managed in GPU memory, transferring visible ones to the GPU just in time, replacing unnecessary ones. The LOD level is selected based on camera distance and memory. Documented inspiration from virtual texturing, preprocessing uses a Python app with JIT optimizations, while a C++ app renders Gaussians in real-time with Vulkan API. We demonstrate its effectiveness in reducing Gaussians, minimizing memory and time for a 3DGS frame render.

We efficiently determine visible Gaussian pages by addressing occlusions with a mesh. While 3DGS involves millions of ellipsoids, making overlap-free grouping difficult, our method groups Gaussians by position. Page linking aligns mesh textures with Gaussians, preventing

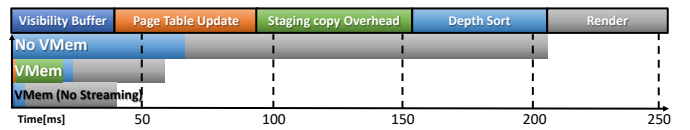


Fig. 23: Time taken to render a frame with the median of each stage on mobile. The last bar displays a fictional frame that is the same as the one above it but with the streaming overhead removed.

discrepancies. LOD shows reduced memory use and improved performance, opening research opportunities. We use virtual texturing to further cut memory and boost performance, vital for expanding 3DGS to larger scenes and aiding industry adoption, especially for mobile devices with integrated GPUs and low hardware needs.

In contrast to related works, we avoid compression in order to put additional stress on our system. Large scene reconstruction is still an active research topic and such tools are not readily available yet. Not compressing Gaussians allows us to test our method at its limits to effectively find shortcomings. We demonstrate the use of virtual texturing in this field, effectively reducing memory and enhancing performance. This is crucial for expanding 3DGS to larger scenes and promoting industry adoption, particularly for applications targeting mobile devices with integrated GPUs and low hardware requirements.

In future work, several shortcomings are subject to further investigation. Our current page linking method corrects artifacts from Gaussians assigned to pages by their mean, but such overlaps are common, increasing the number of required pages. Future work might adjust page assignments to reduce overlaps, or ignore small overlaps without affecting image quality significantly. Our LOD solution, based on Yan *et al.* [39] and mipmapping, serves as a proof of concept showing compatibility with virtual memory. However, it needs improvements to manage abrupt distance changes adaptively LOD, and the merging of Gaussians by a fixed factor doesn't cover them accurately. Popping artifacts during page level changes remain unaddressed. As seen in Section 2, recent research in LOD for 3DGS has gained interest; some approaches could complement our future work.

Our approach avoids Gaussian compression to explore its limitations. Enhanced datasets and algorithms will aid in testing large scenes. Future versions may adopt Gaussian compression through texture algorithms to reduce data copies and apply vector quantization for smaller codebooks in GPU, lessening data transfer. Unlike Kerbl's *et al.* [14] software rasterizer for 3DGS scenes, which sorts Gaussians by tile for potential performance gains, our method is hardware-based, sorting Gaussians by camera distance. Transparency challenges in page determination echo traditional virtual texturing issues (Mayer [23]), crucial for realistic representations in 3DGS with transparencies. A possible solution is to pin pages on transparent surfaces in GPU.

Currently, our method avoids scene reconstruction changes, starting with a complete scene for preprocessing. Future work could integrate virtual memory into the training phase, regularly preprocessing and rendering with visibility determination.

ACKNOWLEDGMENTS

Funded by the European Union under Grant Agreement No. 101092861. Views and opinions expressed are, however, those of the author(s) only and do not necessarily reflect those of the European Union or the European Commission. Neither the European Union nor the granting authority can be held responsible for them..

REFERENCES

- [1] S. Barrett. Sparse virtual textures. <https://silverspaceship.com/src/svt/>, 2008. Accessed: 2024-06-04. 3, 5
- [2] J. T. Barron, B. Mildenhall, D. Verbin, P. P. Srinivasan, and P. Hedman. Zip-nerf: Anti-aliased grid-based neural radiance fields. *ICCV*, 2023. 8
- [3] H. Chen, C. Li, and G. H. Lee. Neug: Neural implicit surface reconstruction with 3d gaussian splatting guidance. (arXiv:2312.00846), Dec. 2023. arXiv:2312.00846 [cs]. 2
- [4] Z. Fan, K. Wang, K. Wen, Z. Zhu, D. Xu, and Z. Wang. Lightgaussian: Unbounded 3d gaussian compression with 15x reduction and 200+ fps. (arXiv:2311.17245), Feb. 2024. arXiv:2311.17245 [cs]. 2

- [5] A. Frumusanu. The 2020 mac mini unleashed: Putting apple silicon m1 to the test. <https://www.anandtech.com/show/16252/mac-mini-apple-m1-tested>, 2020. Accessed: 2024-10-18. 10
- [6] L. Gao, J. Yang, B.-T. Zhang, J.-M. Sun, Y.-J. Yuan, H. Fu, and Y.-K. Lai. Mesh-based gaussian splatting for real-time large-scale deformation. (arXiv:2402.04796), Feb. 2024. arXiv:2402.04796 [cs]. 2
- [7] S. Girish, K. Gupta, and A. Shrivastava. Eagles: Efficient accelerated 3d gaussians with lightweight encodings. (arXiv:2312.04564), Dec. 2023. arXiv:2312.04564 [cs]. 2
- [8] T. K. Group. Khronos vulkan portability initiative. <https://www.khronos.org/vulkan/portability-initiative>, 2024. Accessed: 2024-10-15. 7
- [9] A. Guédon and V. Lepetit. Sugar: Surface-aligned gaussian splatting for efficient 3d mesh reconstruction and high-quality mesh rendering. (arXiv:2311.12775), Dec. 2023. arXiv:2311.12775 [cs]. 2
- [10] J. Haberl. *Virtual memory for 3D Gaussian Splatting*. Master's Thesis, Institute of Visual Computing, Graz University of Technology, Inffeldgasse 16/2, A-8010 Graz, Austria, Dec. 2024. doi: 10.3217/xstz7-q3q02 6
- [11] J. Hable. Variable rate shading with visibility buffer rendering. <https://advances.realtimerendering.com/s2024/index.html#hable>, 2024. Accessed: 2024-08-07. 6
- [12] E. Hartmann. Computerunterstützte darstellende und konstruktive geometrie. <https://www2.mathematik.tu-darmstadt.de/~ehartmann/cdg-skript-1998.pdf>, 1997. Accessed: 2024-09-09. 3
- [13] P. Jiang, G. Pandey, and S. Saripalli. 3dgs-reloc: 3d gaussian splatting for map representation and visual relocalization. (arXiv:2403.11367), Mar. 2024. arXiv:2403.11367 [cs]. 2
- [14] B. Kerbl, G. Kopanas, T. Leimkuehler, and G. Drettakis. 3D Gaussian Splatting for Real-Time Radiance Field Rendering. *ACM Transactions on Graphics*, 42(4):1–14, Aug. 2023. doi: 10.1145/3592433 1, 2, 5, 6, 11
- [15] B. Kerbl, A. Meuleman, G. Kopanas, M. Wimmer, A. Lanvin, and G. Drettakis. A hierarchical 3d gaussian representation for real-time rendering of very large datasets. *ACM Transactions on Graphics*, 43(4):1–15, July 2024. doi: 10.1145/3658160 2, 8, 11
- [16] J. C. Lee, D. Rho, X. Sun, J. H. Ko, and E. Park. Compact 3d gaussian representation for radiance field. (arXiv:2311.13681), Nov. 2023. arXiv:2311.13681 [cs]. 2
- [17] Z. Li, Z. Chen, Z. Li, and Y. Xu. Spacetime gaussian feature splatting for real-time dynamic view synthesis. (arXiv:2312.16812), Dec. 2023. arXiv:2312.16812 [cs]. 2
- [18] J. Lin, Z. Li, X. Tang, J. Liu, S. Liu, J. Liu, Y. Lu, X. Wu, S. Xu, Y. Yan, and W. Yang. Vastgaussian: Vast 3d gaussians for large scene reconstruction. (arXiv:2402.17427), Feb. 2024. arXiv:2402.17427 [cs]. doi: 10.48550/arXiv.2402.17427 2, 8
- [19] L. Lin, Y. Liu, Y. Hu, X. Yan, K. Xie, and H. Huang. Capturing, reconstructing, and simulating: the urbanscene3d dataset. (arXiv:2107.04286), July 2022. arXiv:2107.04286 [cs]. 8
- [20] Y. Liu, H. Guan, C. Luo, L. Fan, N. Wang, J. Peng, and Z. Zhang. Citygaussian: Real-time high-quality large-scale scene rendering with gaussians. (arXiv:2404.01133), July 2024. arXiv:2404.01133 [cs]. doi: 10.48550/arXiv.2404.01133 2
- [21] W. E. Lorensen and H. E. Cline. Marching cubes: A high resolution 3d surface construction algorithm. In *Proceedings of the 14th Annual Conference on Computer Graphics and Interactive Techniques*, SIGGRAPH '87, 7 pages, p. 163–169. Association for Computing Machinery, New York, NY, USA, 1987. doi: 10.1145/37401.37422 2
- [22] T. Lu, M. Yu, L. Xu, Y. Xiangli, L. Wang, D. Lin, and B. Dai. Scaffold-gs: Structured 3d gaussians for view-adaptive rendering. (arXiv:2312.00109), Nov. 2023. arXiv:2312.00109 [cs]. 2
- [23] A. J. Mayer. *Virtual Texturing*. Master's Thesis, Institute of Computer Graphics and Algorithms, Vienna University of Technology, Favoritenstrasse 9-11/E193-02, A-1040 Vienna, Austria, Oct. 2010. 3, 6, 11
- [24] M. Mittring and C. GmbH. Advanced virtual texture topics. In *ACM SIGGRAPH 2008 Games*, SIGGRAPH '08, 29 pages, p. 23–51. Association for Computing Machinery, New York, NY, USA, 2008. doi: 10.1145/1404435.1404438 4
- [25] W. Morgenstern, F. Barthel, A. Hilsmann, and P. Eisert. Compact 3d scene representation via self-organizing gaussian grids. (arXiv:2312.13299), Dec. 2023. arXiv:2312.13299 [cs]. 2
- [26] NanoReview.net. Apple ipad pro 11" (3rd gen. 2021). <https://nanoreview.net/en/tablet/apple-ipad-pro-11-3rd-gen-2021?m=r.1>, 2021. Accessed: 2024-10-18. 10
- [27] K. Navaneet, K. Pourahmadi Meibodi, S. Koohpayegani, and H. Pirsiavash. *Compact3D: Compressing Gaussian Splat Radiance Field Models with Vector Quantization*. Jan. 2024. 2
- [28] S. Niedermayr, J. Stumpfegger, and R. Westermann. Compressed 3d gaussian splatting for accelerated novel view synthesis. (arXiv:2401.02436), Jan. 2024. arXiv:2401.02436 [cs]. 2
- [29] A. Pranckevičius. Making gaussian splats more smaller. <https://aras-p.info/blog/2023/09/27/Making-Gaussian-Splats-more-smaller/>, Sep 2023. Accessed: 2024-04-06. 2
- [30] A. Pranckevičius. Making gaussian splats smaller. <https://aras-p.info/blog/2023/09/13/Making-Gaussian-Splats-smaller/>, Sep 2023. Accessed: 2024-06-04. 2
- [31] K. Ren, L. Jiang, T. Lu, M. Yu, L. Xu, Z. Ni, and B. Dai. Octree-gs: Towards consistent real-time rendering with lod-structured 3d gaussians. (arXiv:2403.17898), Mar. 2024. arXiv:2403.17898 [cs]. 2
- [32] A. Richermoz. Sparse texture binding is painfully slow. <https://forums.developer.nvidia.com/t/sparse-texture-binding-is-painfully-slow>, 2023. Accessed: 2024-09-01. 5
- [33] M. Tancik, E. Weber, E. Ng, R. Li, B. Yi, J. Kerr, T. Wang, A. Kristoffersen, J. Austin, K. Salahi, A. Ahuja, D. McAllister, and A. Kanazawa. Nerfstudio: A modular framework for neural radiance field development. In *ACM SIGGRAPH 2023 Conference Proceedings*, SIGGRAPH '23, 2023. 4, 8
- [34] N. Tatarchuk. Welcome and introduction – trends in games and rendering. <https://advances.realtimerendering.com/s2024/index.html#intro>, 2024. Accessed: 2024-08-20. 7
- [35] techpowerup.com. Nvidia geforce gtx 1070. <https://www.techpowerup.com/gpu-specs/geforce-gtx-1070.c2840>, 2024. Accessed: 2024-10-18. 10
- [36] The Brenwill Workshop Ltd. Moltenvk. <https://github.com/KhronosGroup/MoltenVK>, 2015. Accessed: 2024-09-24. 5
- [37] J. Waczyńska, P. Borycki, S. Tadeja, J. Tabor, and P. Spurek. Games: Mesh-based adapting and modification of gaussian splatting. (arXiv:2402.01459), Feb. 2024. arXiv:2402.01459 [cs]. 2
- [38] S. Willems. Hardware capability database for vulkan. <http://vulkan.gpuinfo.org>, 2016. Accessed: 2024-09-24. 5
- [39] Z. Yan, W. F. Low, Y. Chen, and G. H. Lee. Multi-scale 3d gaussian splatting for anti-aliased rendering. (arXiv:2311.17089), Nov. 2023. arXiv:2311.17089 [cs]. 2, 4, 11
- [40] Y. Yuan, X. Li, Y. Huang, S. De Mello, K. Nagano, J. Kautz, and U. Iqbal. Avatar: Animatable 3d gaussian avatars with implicit mesh learning. (arXiv:2312.11461), Dec. 2023. arXiv:2312.11461 [cs]. 2
- [41] H. Zhao, H. Weng, D. Lu, A. Li, J. Li, A. Panda, and S. Xie. On scaling up 3d gaussian splatting training. (arXiv:2406.18533), June 2024. arXiv:2406.18533 [cs]. 2